

Article

# Hard-core Radius of Nucleons within the Induced Surface Tension Approach

K. A. Bugaev<sup>1</sup>, A. I. Ivanytskyi<sup>1,2</sup>, V. V. Sagun<sup>1,3</sup>, B. E. Grinyuk<sup>1</sup>, D. O. Savchenko<sup>1</sup>, G. M. Zinovjev<sup>1</sup>, E. G. Nikonov<sup>4</sup>, L. V. Bravina<sup>5</sup>, E. E. Zabrodin<sup>5,6,7</sup>, D. B. Blaschke<sup>7,8,9</sup>, A. V. Taranenko<sup>7</sup>, L. Turko<sup>8</sup>

<sup>1</sup> Bogolyubov Institute for Theoretical Physics of the National Academy of Sciences of Ukraine, 03680 Kiev, Ukraine

<sup>2</sup> Department of Fundamental Physics, University of Salamanca, Plaza de la Merced s/n 37008, Spain

<sup>3</sup> Centro de Astrofísica e Gravitação - CENTRA, Departamento de Física, Instituto Superior Técnico, Universidade de Lisboa, 1049-001 Lisboa, Portugal

<sup>4</sup> Laboratory for Information Technologies, Joint Institute for Nuclear Research, Dubna 141980, Russia

<sup>5</sup> Department of Physics, University of Oslo, PB 1048 Blindern, N-0316 Oslo, Norway

<sup>6</sup> Skobel'tzyn Institute of Nuclear Physics, Moscow State University, 119899 Moscow, Russia

<sup>7</sup> National Research Nuclear University "MEPhI" (Moscow Engineering Physics Institute), 115409 Moscow, Russia

<sup>8</sup> Institute of Theoretical Physics, University of Wrocław, pl. M. Borna 9, 50-204 Wrocław, Poland

<sup>9</sup> Bogoliubov Laboratory of Theoretical Physics, JINR Dubna, Joliot-Curie str. 6, 141980 Dubna, Russia

\* Correspondence: \*bugaev@fias.uni-frankfurt.de

Version November 7, 2018 submitted to MDPI

**Abstract:** In this work we discuss a novel approach to model the hadronic and nuclear matter equations of state using the induced surface tension concept. Since the obtained equations of state, classical and quantum, are among the most successful ones in describing the properties of low density phases of strongly interacting matter, they set strong restrictions on the possible value of the hard-core radius of nucleons. Therefore, we perform a detailed analysis of its value which follows from hadronic and nuclear matter properties and find the most trustworthy range of its values: the hard-core radius of nucleons is 0.3–0.36 fm. A comparison with the phenomenology of neutron stars implies that the hard-core radius of nucleons has to be temperature and density dependent.

**Keywords:** quark-hadron phase transition, excluded hadron volume, chemical freeze-out, neutron star matter

## 1. Introduction

A reliable and precise determination of major characteristics of symmetric nuclear matter is of fundamental importance [1–5] not only for the nuclear spectroscopy and for nuclear physics of intermediate energies, but also for nuclear astrophysics in view of possible phase transformations which may occur in compact astrophysical objects such as neutron stars, and hypothetical hybrid and quark stars. Such characteristics of infinite nuclear matter as the normal density  $n_0 \simeq 0.16 \text{ fm}^{-3}$  at zero pressure and zero temperature, its binding energy per nucleon  $W_0 = -16 \text{ MeV}$  and its incompressibility factor  $K_0 \simeq 250 - 315 \text{ MeV}$  [6] are of great importance for various phenomenological approaches, since these characteristics are widely used for determination of the model parameters. Furthermore, such a parameter of the nuclear matter as the hard-core radius (HCR) of nucleons  $R_N$  plays an important role not only in nuclear physics [1,3], but also in nuclear astrophysics [2,4] and in the physics of heavy ion collisions (HIC) [7–16]. However, in the literature one can find any value of  $R_N$  in the range 0.3 – 0.7 fm. Partly the problem is related to the fact that almost all equations of

state (EoS) with the hard-core repulsion employ the Van der Waals (VdW) approximation which is applicable only at low particle number densities.

However, recently a novel and convenient approach to the EoS has been developed which allows one to safely go beyond the VdW approximation for any number of HCR (multicomponent case) [17–20]. Having a single additional parameter compared to the multicomponent VdW EoS this approach enables us to describe on the same footing the data measured in HIC, to reproduce the nuclear matter properties up to five normal nuclear densities and to describe the mass-radius relation of neutron stars. Here we consider the constraints which follow from the proton flow and from the S-matrix approach, and discuss how they allow one to determine the most trustworthy range of  $R_N$  values. We draw some conclusions for developing the EoS of neutron star matter.

The work is organized as follows. In Sect. 2 we recall the main equations of the hadron resonance gas model (HRGM) [18–20] based on the concept of induced surface tension [30]. The new results on the quantum formulation of the induced surface tension equation of state for nuclear matter are discussed in Sect. 3, whereas our conclusions are summarized in Sect. 4.

## 2. Multicomponent formulation of HRGM with hard-core repulsion

For many years the HRGM [7–20] is successfully used to finding out the parameters of chemical freeze-out (CFO) from the hadronic yields measured experimentally in high energy nuclear collisions. Presently the HRGM with multicomponent hard-core repulsion between hadrons [8–12,15–20] gives the most successful description of all independent hadronic multiplicity ratios which have been measured in the heavy ion collisions high energy experiments performed from early 70' (Bevalac) till present over BNL-AGS, GSI-SIS, CERN-SPS, BNL-RHIC to CERN-LHC at the broad center of mass energies  $\sqrt{s_{NN}}$  from 2.7 to 5020 GeV. There exist three major grounds to consider the HRGM with multicomponent hard-core repulsion as the realistic EoS of hadronic matter at high temperatures and moderate particle number densities. Firstly, for a long time it is well known that for temperatures below 170 MeV and moderate baryonic charge densities (below about twice nuclear saturation density) the mixture of stable hadrons and their resonances whose interaction is described by the quantum second virial coefficients behaves almost like a mixture of ideal gases of stable particles which, however, includes both the hadrons and their resonances, but with their averaged vacuum values of masses [21]. As it was demonstrated in Ref. [21], the main physical reason for this kind of behavior is rooted in an almost complete cancellation between the attractive and repulsive terms in the quantum second virial coefficients. Hence, the residual deviation from the ideal gas (a weak repulsion) can be modeled by the classical second virial coefficients.

Secondly, by considering the HRGM as the hadronic matter EoS one can be sure that its pressure will never exceed the one of the quark-gluon plasma. The latter may occur, if the hadrons are treated as the mixture of ideal gases [18,22]. Thirdly, an additional reason to regard the HRGM as hadronic matter EoS in the vicinity of CFO is the practical one: since the hard-core repulsion is a contact interaction, the energy per particle of such an EoS equals to the one of the ideal gas, even for the case of quantum statistics [20]. Therefore, during the evolution of the system after CFO to the kinetic freeze-out one will not face a hard mathematical problem [23,24] to somehow “convert” the potential energy of interacting particles into their kinetic energy and into the masses of particles which appear due to resonance decays.

Apparently, these reasons allow one to consider the HRGM as an extension of the statistical bootstrap model [25] augmented with the hard-core repulsion, but for a truncated hadronic mass-volume spectrum, and to effectively apply it to the description of hadronic multiplicities measured in the heavy ion collision experiments.

Although many valuable findings were obtained with the HRGM during last few years, at the moment the HCR are well established for the most abundant hadrons only, i.e. for pions ( $R_\pi \simeq 0.15 \pm 0.02$  fm), for the lightest  $K^\pm$ -mesons ( $R_K \simeq 0.395 \pm 0.03$  fm), for nucleons ( $R_p \simeq 0.365 \pm 0.03$  fm) and for the lightest (anti) $\Lambda$ -hyperons ( $R_\Lambda \simeq 0.085 \pm 0.015$  fm) [18,19]. Nevertheless, there is a

confidence that in few years from now the new data of high quality which will be measured at RHIC BNL (Brookhaven) [26], NICA JINR (Dubna) [27] and FAIR GSI (Darmstadt) [28], will help us to find out the HCR of other measured hadrons with unprecedentedly high accuracy. However, one should remember that the traditional multicomponent HRGM based on the VdW approximation is not suited for such a purpose, since for  $N \sim 100$  different HCR, where  $N$  corresponds to the various hadronic species produced in a collision, one has to find a solution of  $N$  transcendental equations. Therefore, an increase of the number of HCR to  $N \sim 100$  will lead to hard computational problems for the traditional HRGM with multicomponent hard-core repulsion. To resolve this principal problem the new HRGM based on the induced surface tension (IST) concept [30] was recently developed in Refs. [18–20].

The IST EoS is a system of two coupled equations for the pressure  $p$  and the IST coefficient  $\Sigma$

$$p = \sum_{k=1}^N p_k = T \sum_{k=1}^N \phi_k \exp \left[ \frac{\mu_k}{T} - \frac{4}{3} \pi R_k^3 \frac{p}{T} - 4\pi R_k^2 \frac{\Sigma}{T} \right], \quad (1)$$

$$\Sigma = \sum_{k=1}^N \Sigma_k = T \sum_{k=1}^N R_k \phi_k \exp \left[ \frac{\mu_k}{T} - \frac{4}{3} \pi R_k^3 \frac{p}{T} - 4\pi R_k^2 \frac{\Sigma}{T} \right], \quad (2)$$

$$\mu_k = \mu_B B_k + \mu_{I3} I_{3k} + \mu_S S_k, \quad (3)$$

where  $\alpha = 1.245$ , and  $\mu_B, \mu_S, \mu_{I3}$  are the chemical potentials of baryon number, the strangeness, and the third projection of the isospin, respectively. Here  $B_k, S_k, I_{3k}, m_k$  and  $R_k$  denote, respectively, the corresponding charges, mass, and HCR of the  $k$ -th hadronic species. The sums in Eqs. (1) and (2) run over all hadronic species including their antiparticles which are considered as independent species. Therefore,  $p_k$  and  $\Sigma_k$  are, respectively, the partial pressure and the partial induced surface tension coefficient of the  $k$ -th hadronic species.

In Eqs. (1) and (2) the thermal density  $\phi_k$  of the  $k$ -th hadronic sort contains the Breit-Wigner mass attenuation. Hence, in the Boltzmann approximation (the quantum gases are discussed in Ref. [20]) it can be cast

$$\phi_k = g_k \gamma_S^{|s_k|} \int_{M_k^{Th}}^{\infty} \frac{dm}{N_k(M_k^{Th})} \frac{\Gamma_k}{(m - m_k)^2 + \Gamma_k^2/4} \int \frac{d^3 p}{(2\pi)^3} \exp \left[ -\frac{\sqrt{p^2 + m^2}}{T} \right]. \quad (4)$$

Here  $g_k$  is the degeneracy factor of the  $k$ -th hadronic species,  $\gamma_S$  is the strangeness suppression factor [29],  $|s_k|$  is the number of valence strange quarks and antiquarks in this hadron species, and the quantity  $N_k(M_k^{Th}) \equiv \int_{M_k^{Th}}^{\infty} \frac{dm \Gamma_k}{(m - m_k)^2 + \Gamma_k^2/4}$  denotes a normalization factor with  $M_k^{Th}$  being the decay threshold mass of the  $k$ -th hadronic sort, while  $\Gamma_k$  denotes its width.

To employ the system of Eqs. (1), (2), and (3) to an investigation of heavy ion collisions one has to supplement it by the strange charge conservation condition

$$n_S \equiv \frac{\partial p}{\partial \mu_S} = \sum_k S_k n_k = 0, \quad (5)$$

which provides a vanishing net strange charge. Here  $n_k$  is the particle number density of hadrons of sort  $k$  defined by the following system of equations

$$n_k \equiv \frac{\partial p}{\partial \mu_k} = \frac{1}{T} \cdot \frac{p_k a_{22} - \Sigma_k a_{12}}{a_{11} a_{22} - a_{12} a_{21}}, \quad a_{11} = 1 + \frac{4}{3} \pi \sum_k R_k^3 \frac{p_k}{T}, \quad a_{12} = 4\pi \sum_k R_k^2 \frac{p_k}{T}, \quad (6)$$

$$a_{22} = 1 + 4\pi \alpha \sum_k R_k^2 \frac{\Sigma_k}{T}, \quad a_{21} = \frac{4}{3} \pi \sum_k R_k^3 \frac{\Sigma_k}{T}. \quad (7)$$

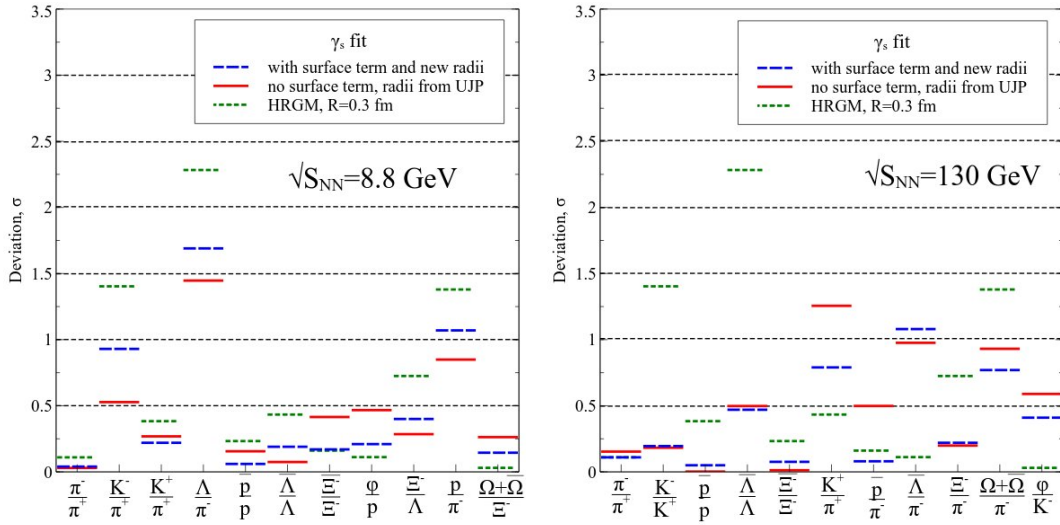


**Figure 1.** Deviations of theoretically predicted hadronic yield ratios from experimental values in units of experimental error  $\sigma$  are shown for the center of mass collision energies  $\sqrt{s_{NN}} = 8.8$  GeV and  $\sqrt{s_{NN}} = 130$  GeV. Dashed lines correspond to the IST EoS fit, while the solid lines correspond to the original HRGM fit [11]. For a comparison the results obtained by the HRGM1 with a single hard-core radius  $R_{all} = 0.3$  fm for all hadrons are also shown (for more details see text).

In contrast to the traditional multicomponent HRGM formulations to determine the particle number densities  $\{n_k\}$  one needs to solve only a system of three equations, i.e. Eqs. (1), (2) and (5), irrespective to the number of different HCR in the EoS. Hence, we believe that the IST EoS given by the system (1)-(5) is well suited for the analysis of all hadronic multiplicities which will be measured soon at RHIC, NICA and FAIR.

Compared to the VdW EoS, the IST EoS has another great advantage of the IST EoS, since it is valid up to the packing fractions  $\eta \equiv \sum_k \frac{4}{3} \pi R_k^3 n_k \simeq 0.2$  [18–20] at which the VdW approximation employed in the traditional HRGM [7–12] becomes completely incorrect (see a discussion below).

From the particle number density (6) of the  $k$ -th species of hadrons one can find out their thermal  $N_k^{th} = V n_k$  ( $V$  is the effective volume of CFO hyper-surface) and total multiplicity  $N_k^{tot}$ . The total multiplicity  $N_k^{tot}$  accounts for the hadronic decays after the CFO and, hence, the ratio of total hadronic multiplicities at CFO can be written

$$\frac{N_k^{tot}}{N_j^{tot}} = \frac{n_k + \sum_{l \neq k} n_l Br_{l \rightarrow k}}{n_j + \sum_{l \neq j} n_l Br_{l \rightarrow j}}. \quad (8)$$

Here  $Br_{l \rightarrow k}$  denotes the branching ratio, i.e., a probability of particle  $l$  to decay strongly into a particle  $k$ . Further details on the actual fitting procedure of experimental hadronic multiplicities by the HRGM can be found in [11,18].

The parameter  $\alpha = 1.25$  was fixed in Refs. [18,19], since this value allows us to simultaneously reproduce the third and fourth virial coefficients of the gas of classical hard spheres. Such a formulation of the IST EoS is used to simultaneously fit 111 independent hadron yield ratios measured at AGS, SPS and RHIC energies. In this fit the factor  $\gamma_s$  and the chemical potentials  $\mu_B$  and  $\mu_{I3}$  are regarded as the free parameters and we found that the best description of these data is reached for the following HCR of baryons  $R_b = 0.365 \pm 0.03$  fm, mesons  $R_m = 0.42 \pm 0.04$  fm, pions  $R_\pi = 0.15 \pm 0.02$  fm, kaons  $R_K = 0.395 \pm 0.03$  fm and  $\Lambda$ -hyperons  $R_\Lambda = 0.085 \pm 0.015$  fm (new radii hereafter). These values of the HCR generate  $\chi_1^2/dof = 57.099/50 \simeq 1.14$  [19]. Some selected results of this fit are shown in Figs. 1, 2.

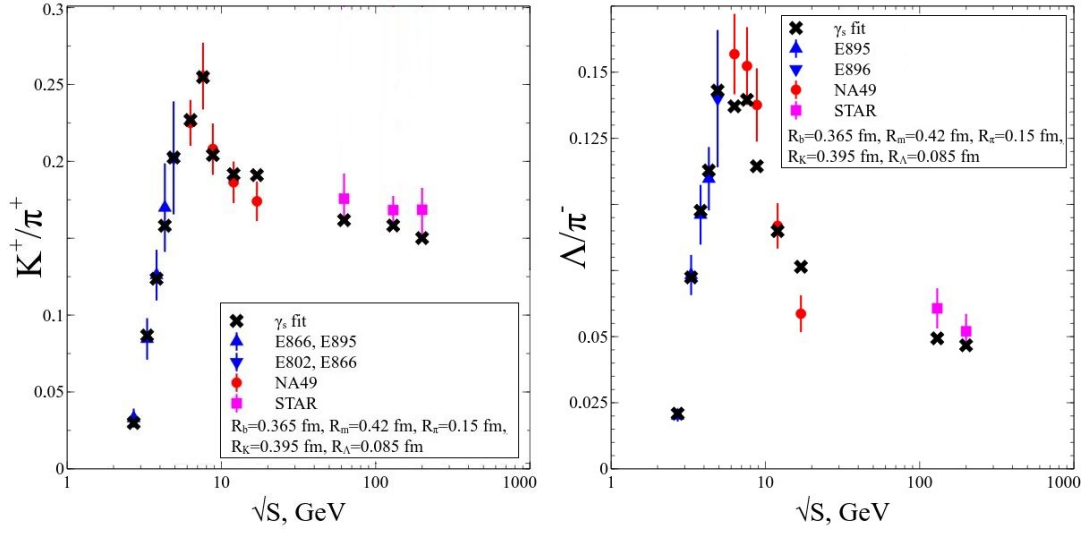


**Figure 2.** The fit results obtained by the IST EoS:  $\sqrt{s_{NN}}$  dependence of  $K^+/\pi^+$  (left panel) and  $\Lambda/\pi^-$  (right panel) ratios. For more than a decade these ratios were the most problematic one to reproduce by the HRGM.

The found HCR were fixed and then used to fit 11 independent hadron yield ratios measured by the ALICE Collaboration (for details see [18,19]) with a single fitting parameter, namely the CFO temperature, since all the chemical potentials were set to zero, while the factor  $\gamma_s$  was set to 1. The fit quality  $\chi^2/dof \simeq 8.92/10 \simeq 0.89$  of the ALICE data is similar to the one found for the combined fit of the AGS, SPS and RHIC data (see Fig. 3). Therefore, the combined quality of the AGS, SPS, RHIC and ALICE data description achieved by the IST EoS [19] is  $\chi^2_{tot}/dof \simeq 66.02/60 \simeq 1.1$ .

In order to show the importance of the multicomponent hard-core repulsion in Fig. 1 the obtained results are compared to the HRGM with a single HCR of hadrons  $R_{all} = 0.3$  fm (HRGM1 hereafter). The HRGM1 employs the quantum statistics for all hadrons and, hence, it is similar to the model of Ref. [7]. The main differences with Refs. [7,13] are: the HRGM1 includes the widths of all hadronic resonances for all temperatures and it is used to fit not all hadronic ratios, but only the independent ones. Such a comparison with the multicomponent versions of HRGM is necessary in order to illustrate the disadvantages of the one component case compared to the multicomponent formulation. The fit quality obtained by the HRGM1 for AGS, SPS and RHIC energies is  $\chi^2_1/dof = 75.134/54 \simeq 1.39$  [19] which is essentially worse compared to the IST results. For this case the value of common HCR was not fitted and, hence, the number of degrees of freedom for HRGM1 is 54. Using the HRGM1 to fit the ALICE data we obtained the fit quality  $\chi^2_2/dof \simeq 12.4/10 \simeq 1.24$  [19]. Hence, the quality of the combined fit for all energies with the HRGM1 is  $\chi^2_{tot}/dof \simeq 87.53/64 \simeq 1.37$ , i.e., it is worse than the one found for the multicomponent IST EoS.

These results clearly demonstrate that additional 3 or 4 HCR can, indeed, essentially improve the quality of the fit of more than hundred independent hadron multiplicity ratios and, hence, such an improvement provides a high confidence in the extracted parameters of CFO. Apparently, this is also a strong argument in favor of  $R_N = 0.365 \pm 0.03$  fm found by the IST EoS. Moreover, from the left panel of Fig. 1 one can see that the proton to negative pion ratio cannot be described within the HRGM1, while it is well described within either of the HRGM multicomponent formulations.

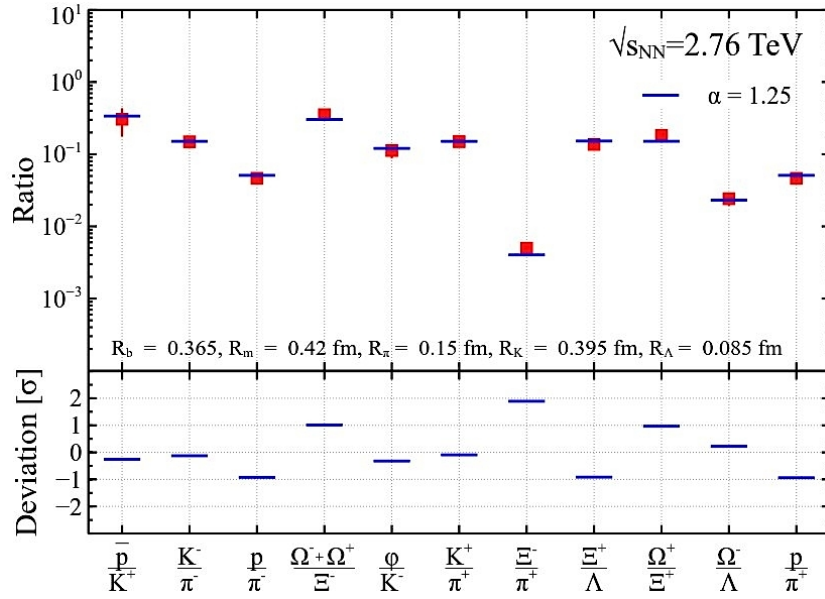


**Figure 3.** The results obtained by the IST EOS on fitting the ALICE data with the new HCR found in [18] from fitting the AGS, SPS and RHIC data. The found CFO temperature is  $T_{CFO} \simeq 148 \pm 7$  MeV. The fit quality is  $\chi^2/dof \simeq 8.92/10 \simeq 0.89$ . The upper panel shows the fit of the ratios, while the lower panel shows the deviation between data and theory in units of estimated error.

### 3. Nuclear Matter IST EoS and Proton Flow Constraint

Now we turn to a discussion the quantum version of the IST EoS used to model the nuclear liquid-gas phase transition. The model pressure  $p$  is a solution of the system ( $R_N$  is the HCR on nucleons)

$$p = p_{id}(T, \nu_p) - p_{int}(n_{id}(T, \nu_p)), \quad (9)$$

$$\Sigma = R_N p_{id}(T, \nu_\Sigma), \quad (10)$$

where the grand canonical pressure  $p_{id}(T, \nu)$  and particle number density  $n_{id}(T, \nu) = \frac{\partial p_{id}}{\partial \nu}$  of noninteracting point-like fermions are given by the expressions [31]

$$p_{id} = T g_N \int \frac{d^3 p}{(2\pi)^3} \ln \left[ 1 + \exp \left( \frac{\nu - \sqrt{p^2 + m^2}}{T} \right) \right], \quad n_{id} = g_N \int \frac{d^3 p}{(2\pi)^3} \left[ \exp \left( \frac{\sqrt{p^2 + m^2} - \nu}{T} \right) + 1 \right]^{-1}. \quad (11)$$

Here the system temperature is  $T$ ,  $m_N = 940$  MeV is the nucleon mass and the nucleon degeneracy factor is  $g_N = 4$ .

The term  $-p_{int}$  in Eq. (9) represents the mean-field contribution to the pressure generated by an attraction between the nucleons. Clearly, the repulsive scattering channels are also present in nuclear matter. However, at densities below  $n_{max} \simeq 0.8 \text{ fm}^{-3}$ , which is the maximal density of the flow constraint [32], the repulsion is suppressed, since at these particle number densities the mean nucleon separation is larger than  $r_{min} = \left( \frac{3}{4\pi n_{max}} \right)^{1/3} \simeq 0.7$  fm. But at such distances the microscopic nucleon-nucleon potential is attractive [33], whereas the remaining repulsive interaction can be safely accounted by the particle hard-core repulsion.

The quantity  $\Sigma$  in Eq. (10) is a one-component analog of the IST coefficient of Eq. (2) first introduced in Ref. [30] in order to distinguish it from the eigensurface tension of ordinary nuclei. Here it is appropriate to explain that the IST appears because the virial expansion of the pressure includes



the terms which are proportional not only to the eigenvolume  $V_0 = \frac{4\pi}{3} R_N^3$ , but also to the eigensurface  $S_0 = 4\pi R_N^2$  of a particle with the HCR  $R_N$  [30]. This surface term contribution is just accounted by the IST coefficient  $\Sigma$ . The meaning of  $\Sigma$  as the surface tension coefficient can be easily seen from the effective chemical potentials which are related to the baryonic chemical potential  $\mu$  as

$$v_p = \mu - pV_0 - \Sigma S_0 + U(n_{id}(T, v_p)), \quad (12)$$

$$v_\Sigma = \mu - pV_0 - \alpha \Sigma S_0 + U_0. \quad (13)$$

Here  $\Sigma$  is conjugated to  $S_0$ , while the attractive mean-field potentials are denoted as  $U(n_{id}(T, v_p))$  and  $U_0 = const$ . From these expressions one can conclude that the effects of hard-core repulsion are only partly accounted by the eigenvolume of particles, while the rest is determined by their eigensurface and the IST coefficient  $\Sigma$  (for more details see [30]). Note that the presence of the pressure of point-like particles  $p_{id}$  in Eqs. (9) - (10) is a typical feature of EoSs formulated in the Grand Canonical Ensemble.

The system (9)-(13) is a concrete realization of the quantum model suggested in [20]. The self-consistency condition

$$p_{int}(n) = n U(n) - \int_0^n dn' U(n'), \quad (14)$$

relates the interaction pressure  $p_{int}(n_{id}(T, v_p))$  and the corresponding mean-field potential  $U(n_{id}(T, v_p))$  and it guarantees the fulfillment of all thermodynamic identities [20] for the quantum IST (QIST) EoS.

It is necessary to stress that substituting the constant potential  $U_0(n_{id}(T, v_\Sigma)) = const$  into the consistency condition (14), one automatically finds that the corresponding mean-field pressure should vanish, i.e.  $\tilde{p}_{int}(n_{id}(T, v_\Sigma)) = 0$ . Note also that different density dependences of the attractive mean-field potentials  $U(n_{id})$  and  $U_0$  simply reflect the different origins of their forces. Thus,  $U(n_{id})$  is generated by the bulk part of interaction, while  $U_0$  is related to the surface part. The meaning of  $U_0$  potential can be better understood after the non-relativistic expansion of the nucleon energy  $\sqrt{m^2 + p^2} \simeq m + \frac{p^2}{2m}$  staying in the momentum distribution function of Eq. (11):  $U_0$  lowers the nucleon mass to the value  $m - U_0$  which is similar to the relativistic mean-field approach. The particle number density from the usual thermodynamic identity

$$n_N = \frac{\partial p}{\partial \mu} = \frac{n_{id}(T, v_p)}{1 + V_0 n_{id}(T, v_p) + \frac{3 V_0 n_{id}(T, v_\Sigma)}{1 + 3(\alpha - 1)V_0 n_{id}(T, v_\Sigma)}}. \quad (15)$$

To be specific the power form of the mean-field potential [31] motivated by Ref. [34]

$$U(n_N) = C_d^2 n_N^\kappa \quad \Rightarrow \quad p_{int}(n_N) = \frac{\kappa}{\kappa + 1} C_d^2 n_N^{\kappa+1}, \quad (16)$$

is used. Here the mean-field contribution to the pressure  $p_{int}(n_N)$  is found from the consistency condition (14). This is one of the simplest choices of the mean-field potential which includes two parameters only, i.e.  $C_d^2$  and  $\kappa$ . Since the parameter  $\alpha$  is fixed already (see preceding section), the other two parameters of the QIST model are the hard-core radius  $R_N$  and the constant potential  $U_0$ .

The QIST EoS with four adjustable parameters is able to simultaneously reproduce the main properties of symmetric nuclear matter, i.e. a vanishing pressure  $p_N = 0$  at zero temperature  $T = 0$  and the normal nuclear particle number density  $n_0 = 0.16 \text{ fm}^{-3}$  and the value of its binding energy per nucleon  $W_0 = \frac{\epsilon_N}{n_N} - m = -16 \text{ MeV}$  (where  $\epsilon_N$  is the energy density). Hence, the baryonic chemical potential of nucleons is  $\mu = 923 \text{ MeV}$ . The QIST EoS with the attraction term (16) was normalized to these properties of nuclear matter ground state and, simultaneously, it was fitted [31] to obey the proton flow constraint [32]. In the present analysis we consider a few values of parameter  $\kappa = 0.1, 0.15, 0.2, 0.25$ . For each value of parameter  $\kappa$  the two curves in the  $n_N - p$  plane were found in such a way that the upper curve is located not above the upper branch of the flow constraint, while

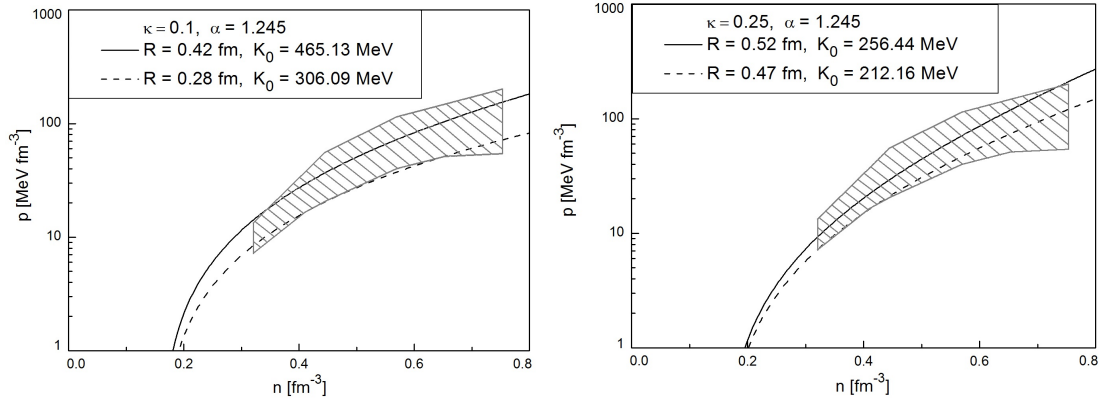


**Figure 4.** Density dependence of the system pressure is shown for several set of parameters which are specified in the legend of each panel. See Table I for more details. The dashed area corresponds to the proton flow constraint of Ref. [32]

**Table 1.** Different sets of parameters which simultaneously reproduce the properties of normal nuclear matter ( $p = 0$  and  $n = n_0 = 0.16 \text{ fm}^{-3}$  at  $\mu = 923 \text{ MeV}$ , see text for details) and obey the proton flow constraint on the nuclear matter EoS along with incompressibility factor  $K_0$  and parameters of CEP.  $R_N, C_d^2, U_0$  and  $\kappa$  are the adjustable parameters of QIST EoS.

	$\kappa = 0.1$		$\kappa = 0.15$		$\kappa = 0.2$		$\kappa = 0.25$	
$R_N$ [fm]	0.28	0.42	0.35	0.48	0.41	0.50	0.47	0.52
$C_d^2$ [MeV · fm <sup>3κ</sup> ]	284.98	325.06	206.05	229.57	168.15	179.67	146.97	152.00
$U_0$ [MeV]	567.32	501.65	343.93	312.83	231.42	217.76	162.03	157.41
$K_0$ [MeV]	306.09	465.13	272.55	405.97	242.56	322.80	217.16	256.44

the lower curve is located not below the lower branch of this constraint. The details are clear from two panels of Fig. 4. Notice that this is highly nontrivial result for an EoS with only four adjustable parameters, since to parameterize the proton flow constraint alone one needs at least 8 independent points! For a comparison we mention that in Ref. [5] it is shown that only 104 of relativistic mean-field EoSs out of 263 analyzed in there are able to obey the proton flow constraint [32] despite the fact that they have 10 or even more adjustable parameters.

However, as was demonstrated in Ref. [35], the lower bound of the proton flow constraint would correspond to a sequence of neutron stars with a maximum mass of only  $\sim 1 M_\odot$  and thus would not fulfill the constraint from the observed mass of  $2.01 \pm 0.04 M_\odot$  for pulsar PSR J0348+432 [36]. In Ref. [35] it was also shown that an equation of state which should fulfill the constraint on the maximum mass should follow the upper bound of the flow constraint. Thus the IST EoS in the parametrization optimized for explaining particle yields from heavy-ion collisions would be too soft for the phenomenology of neutron stars, i.e. at  $T = 0$ . This was noticed recently in Ref. [37].

The values of parameter  $\kappa$  above 0.33 were not considered, since a good description of the proton flow constraint cannot be achieved for  $\kappa \geq 0.33$  [31]. On the other hand, the values of parameter  $\kappa$  below 0.1 were not considered too since they correspond to unrealistically large values of the incompressibility constant  $K_0 \equiv 9 \frac{\partial p}{\partial n_N} \Big|_{T=0, n_N=n_0}$ . As one can find from Table I for  $\kappa = 0.1$  the minimal value of the incompressibility constant  $K_0$  is about 306 MeV, while for  $\kappa < 0.1$  it is even larger.

From Table I one can see that the range of  $R_N$  is still wide, i.e.  $R_N \in [0.28; 0.52]$  fm. The QIST EoS, however, allows one to obtain an essentially narrower range of the nucleon HCR  $R_N$ . Indeed, if one requires that this EoS should be applicable at the maximal value of particle number density  $n_{max} \simeq 0.8 \text{ fm}^{-3}$  of the proton flow constraint, then such a condition can be written as

$$\frac{4}{3} \pi R_N^3 n_{max} \leq \eta_{max}. \quad (17)$$



Here the range of the QIST EoS applicability is given by the maximal packing fraction  $\eta_{max}$  of the model. Assuming that the maximal packing fraction of the QIST EoS is  $\eta_{max} = 0.2$ , i.e. it is similar to the Boltzmann version of the IST EoS [18,19], one gets the following inequality on the nucleon hard-core radius  $R_N \leq 0.4$  fm and, hence, one finally obtains  $0.28 \text{ fm} \leq R_N \leq 0.4 \text{ fm}$ .

The quantum virial expansion developed in [20] both for the quantum VdW and QIST EoS allows us to obtain even a narrower range of values which is consistent with the S-matrix approach [38] to the EoS of the gas of nucleons at temperatures above 100 MeV. For an extended discussion see also Ref. [39]. In particular, the quantum second virial coefficient  $a_2^S(T)$  of a nucleon gas as obtained from realistic S-matrix approach provides approximately the following inequalities [38,39]

$$0.5 \text{ fm}^3 \leq a_2^S(T) \leq 1.25 \text{ fm}^3 \quad \text{for} \quad 100 \text{ MeV} \leq T \leq 170 \text{ MeV}. \quad (18)$$

These inequalities correspond to the conditions  $0.31 \text{ fm} \leq R_N \leq 0.42 \text{ fm}$ , if one uses the classical definition of the HCR. It is interesting that these inequalities are similar to the ones found above for the QIST EoS. Using the results of Ref. [20] the second  $a_2^{IST}$  and third  $a_3^{IST}$  virial coefficients for the repulsive part of the QIST EoS for nucleons can be cast as

$$a_2^{IST} = 4V_0 + a_2^{(0)}, \quad a_3^{IST} \simeq [16 - 18(\alpha - 1)]V_0^2 + 5V_0a_2^{(0)} + a_3^{(0)}, \quad (19)$$

where the second  $a_2^{(0)}$  and the third  $a_3^{(0)}$  virial coefficients of point-like nucleons which in the non-relativistic approximation for fermions can be written as

$$a_2^{(0)} \simeq 2^{-\frac{5}{2}}\omega_N \simeq 0.177\omega_N, \quad a_3^{(0)} \simeq 2 \left[ 2^{-4} - 3^{-\frac{5}{2}} \right] \omega_N^2 \simeq -3.4 \cdot 10^{-3} \omega_N^2, \quad \omega_N = \frac{1}{g_N} \left[ \frac{2\pi\hbar^2}{Tm_N} \right]^{\frac{3}{2}}. \quad (20)$$

Introducing an effective second virial coefficient of nucleons  $a_2^{eff}(n_N) \equiv a_2^{IST} + n_N a_3^{IST}$  which depends on particle number density of nucleons  $n_N$  and assuming that the nucleonic contribution to the HRGM is given by the repulsive part of the QIST EoS (9), one can use the effective second virial coefficient  $a_2^{eff}(n_N)$  to constrain the values of HCR further. Our analysis shows that for the nucleon densities below  $n_N \simeq 3n_0 = 0.48 \text{ fm}^{-3}$  the fourth and higher virial coefficients are not important and, hence, we can require that up to this nucleon density the coefficient  $a_2^{eff}(n_N)$  obeys the constraint (18). This leads to the follows range of  $R_N$  values:  $R_N \in [0.275; 0.36] \text{ fm}$ . In other words, for such a range of values of the nucleonic HCR not only the second, but also the third virial coefficient of nucleons will provide the fulfillment of the constraint (18).

At first glance this result may look surprising, since one does not see any important role of the quantum third virial coefficient. A close inspection shows that due to the small value of the coefficient which enters the expression for  $a_3^{(0)}$ , the quantum effects are important at temperatures below 20 MeV, while at  $T \geq 100 \text{ MeV}$  the coefficients  $a_3^{(0)}$  and  $a_2^{(0)}$  are small, since  $\omega_N(T = 100 \text{ MeV}) \simeq 1$  and it is a decreasing function of  $T$ . As a result at  $T \geq 100 \text{ MeV}$  the values of the coefficients  $a_2^{IST}$  and  $a_3^{IST}$  are defined by the HCR of nucleons and the parameter  $\alpha$ .

However, when the QIST EoS is required to simultaneously fulfill the gravitational mass-radius relation of neutron stars and the proton flow constraint, one finds somewhat larger values of the HCR of nucleons, namely  $R_N \in [0.42; 0.47] \text{ fm}$  [37]. Note that within the recent excluded nucleon volume generalization of the relativistic meanfield model "DD2" by Typel [40] even larger values of the HCR of nucleons were used in the description of neutron star phenomenology such as mass-radius relations [41], moment of inertia [42], tidal deformabilities [42,43] and cooling [44]. The "DD2\_p40" EoS used in these works would correspond to a nucleon HCR of  $R_N = 0.62 \text{ fm}$  which is at the very limit of what is compatible with the recent constraint on the compactness of neutron stars stemming from the gravitational wave signal measured for the inspiral phase of the neutron star merger GW170817 [45]. These results indicate that the repulsive core of the nucleon-nucleon interaction

depends on the properties of the medium since the description of static neutron star properties at zero temperature require a stiffer EoS than the one which is successfully reproducing the hadronic multiplicities measured in HIC. What is the physical reason for such a difference?

It has been demonstrated that the repulsive part of effective density-dependent interactions of the Skyrme type (e.g., the one by Vautherin and Brink [46]) can be reproduced by the quark exchange interaction between nucleons (quark Pauli blocking) [47] in analogy to the hard-sphere model of molecular interactions which is based on the electron exchange interaction among atoms (see, e.g., Ebeling et al. [48]) which is captured, e.g., in the Carnahan-Starling EoS [49]. The repulsive Pauli blocking effect between composite particles is especially pronounced at low temperatures, in the regime of quantum degeneracy.

Note that the QIST model offers a simple way to make a stiffer EoS at higher pressures or densities. Actually, as it was mentioned in the first paper on IST EoS [30], the parameter  $\alpha$  may, in principle, be a function which depends on the system pressure. Therefore, it would be interesting to generalize the QIST EoS and to include into it the pressure or density dependence of the parameter  $\alpha$  and/or of the HCR of nucleons. Then having more adjustable parameters and adding more astrophysical constraints as, e.g., for an upper limit on the maximum mass as well as lower and upper bounds on the neutron star radius from the binary neutron star merger, one could aim at a best possible description including the proton flow constraint and to find a realistic functional dependence of  $\alpha$  and  $R_N$  on density and temperature. In this respect we would like to mention the possibility to model the excluded nucleon volume in a density and temperature dependent way, even changing the sign so that also attractive interactions are accessible. In this form, Typels excluded volume model [40] has been used to obtain an equation of state and phase diagram with a second critical endpoint (CEP) beyond the gas - liquid one [50]. This could be used to mimic effects of the nuclear-to-quark matter phase transition in the QCD phase diagram. Within the IST approach the IST coefficient  $\Sigma$  stands for attraction effects and therefore the interplay of attraction and repulsion as captured in the (medium dependent) parameters  $\alpha$  and  $R_N$ , respectively, could eventually lead to similar behaviour and a second CEP in the phase diagram.

#### 4. Conclusions

Here we thoroughly discussed the IST approach to model the EoS of hadronic and nuclear matter and analyzed different constraints on the HCR of nucleons. The most successful formulation of HRGM gives us  $R_N \simeq 0.365 \pm 0.03$  fm, while the QIST EoS of nuclear matter leads to  $R_N \simeq 0.34 \pm 0.06$  fm. At the same time a comparison of quantum virial coefficients with with S-matrix approach gives us  $R_N \simeq 0.32 \pm 0.04$  fm. Therefore, the most probable range of HCR of nucleons which is consistent with different constraints following from the hadronic and nuclear matter properties is  $R_N \in [0.3; 0.36]$  fm. Since applications of the QIST EoS to the neutron star properties require somewhat larger HCR of nucleons [37], we conclude that the QIST EoS for neutron stars should be improved further, especially an interaction between nucleons at high particle number densities which are typical for the neutron stars core. The generalized QIST EoS which considers the density and temperature dependence of the parameters  $\alpha$  and  $R_N$  may provide a very effective way to solve this problem.

**Acknowledgments:** The authors are thankful to I. N. Mishustin, R. D. Pisarski and S. A. Moszkowski for fruitful discussions and valuable comments. The work of K.A.B., A.I.I., V.V.S., B.E.G., D.O.S. and G.M.Z. was supported by the grants launched by the Section of Nuclear Physics of National Academy of Sciences of Ukraine. V.V.S. thanks the Fundação para a Ciência e Tecnologia (FCT), Portugal, for the financial support through the Grant No. UID/FIS/00099/2013 to make research at the Centro de Astrofísica e Gravitação (CENTRA), Instituto Superior Técnico, Universidade de Lisboa. The work of L.V.B. and E.E.Z. was supported by the Norwegian Research Council (NFR) under grant No. 255253/F50 - CERN Heavy Ion Theory. L.V.B. and K.A.B. thank the Norwegian Agency for International Cooperation and Quality Enhancement in Higher Education for financial support, grant 150400-212051-120000 «CPEA-LT-2016/10094 From Strong Interacting Matter to Dark Matter». D.B.B. is grateful to the COST Action CA15213 “THOR” for networking support and to the MEPhI Academic Excellence program grant No 02.a03.21.0005 for partial support. D.B.B. and L.T. acknowledge support from the Polish National Science Centre (NCN) under grant no. UMO-2014/13/B/ST9/02621. The work of A.V.T. was partially supported by the Ministry of Science and Education of the Russian Federation, grant No. 3.3380.2017/4.6, and by National Research Nuclear University “MEPhI” in the framework of the Russian Academic Excellence Project (contract no.

02.a03.21.0005, 27.08.2013). The work of A.I.I. was done within the project SA083P17 of Universidad de Salamanca launched by the Regional Government of Castilla y Leon and the European Regional Development Fund.

## References

1. H. Stöcker and W. Greiner, Phys. Rep. **1986**, 137, 227
2. J. M. Lattimer, Annu. Rev. Nucl. Part. Sci. **2012**, 62, 485 and references therein.
3. N. Buyukcizmeci, A. S. Botvina, I. N. Mishustin, Astrophys. J. **789**, 33 (2014).
4. S. Benic, D. Blaschke, D. E. Alvarez-Castillo, T. Fischer and S. Typel, Astron. Astrophys. **2015**, 577, A40
5. M. Dutra et al., Phys. Rev. C **2014**, 90, 055203 and references therein.
6. J. R. Stone, N. J. Stone and S. A. Moszkowski, Phys. Rev. C **2014**, 89, 044316
7. A. Andronic, P. Braun-Munzinger and J. Stachel, Nucl. Phys. A **2006**, 772, 167
8. D. R. Oliinychenko, K. A. Bugaev and A. S. Sorin, Ukr. J. Phys. **2013**, 58, 211
9. K. A. Bugaev, D. R. Oliinychenko, A. S. Sorin, G. M. Zinovjev, Eur. Phys. J. A **2013**, 49, 30
10. K. A. Bugaev et al., Europhys. Lett. **2013**, 104, 22002
11. V. V. Sagun, Ukr. J Phys. **2014**, 59, 755
12. V. V. Sagun et al., Ukr. J. Phys. **2014**, 59, 1043
13. J. Stachel, A. Andronic, P. Braun-Munzinger and K. Redlich, J. Phys. Conf. Ser. **2014**, 509, 012019 and references therein.
14. K. A. Bugaev et al., Ukr. J. Phys. **2016**, 61, 659 and references therein
15. K. A. Bugaev et al., Phys. Part. Nucl. Lett. **2015**, 12, 238
16. K. A. Bugaev et al., Eur. Phys. J. A **2016**, 52, 175; and Eur. Phys. J. A **2016**, 52, 227
17. K. A. Bugaev et al., Phys. Part. Nucl. Lett. **2018**, 15, 210
18. K. A. Bugaev et al., Nucl. Phys. A **2018**, 970, 133
19. V. V. Sagun et al., Eur. Phys. J. A **2018**, 54, 100
20. K. A. Bugaev, A. I. Ivanytskyi, V. V. Sagun, E. G. Nikonov and G. M. Zinovjev, arXiv:1704.06846 [nucl-th] (to appear in Ukr. J Phys. (2018)) and references therein
21. R. Venugopalan and M. Prakash, Nucl. Phys. A **1992**, 546, 718
22. L. M. Satarov, M. N. Dmitriev and I. N. Mishustin, Phys. Atom. Nucl. **2009**, 72, 1390
23. K. A. Bugaev, Nucl. Phys. A **1996**, 606, 559
24. K. A. Bugaev, Phys. Rev. Lett. **2003**, 90, 252301 and references therein
25. R. Hagedorn, Nuovo Cim. Suppl. **1965**, 3, 147
26. L. Adamczyk et al., [STAR Collaboration], Phys. Rev. C **2016**, 93, 021903
27. P. Senger, Eur. Phys. J. A **2016**, 52, 217 and references therein
28. P. Senger, Nucl. Phys. A **2011**, 862-863, 139 and references therein
29. J. Rafelski, Phys. Lett. B **1991**, 62, 333
30. V. V. Sagun, A. I. Ivanytskyi, K. A. Bugaev and I. N. Mishustin, Nucl. Phys. A **2014**, 924, 24
31. A. I. Ivanytskyi, K. A. Bugaev, V. V. Sagun, L. V. Bravina and E. E. Zabrodin, Phys. Rev. C **2018**, 97, 064905
32. P. Danielewicz, R. Lacey and W. G. Lynch, Science **2002**, 298, 1593
33. F. Gross, J. W. Van Orden and K. Holinde, Phys. Rev. C **1992**, 45, 2094 and references therein
34. M. I. Gorenstein et al., J. Phys. G **1993**, 19, 69
35. T. Klahn et al., Phys. Rev. C **2006**, 74, 035802
36. J. Antoniadis et al., Science **2013**, 340, 1233232
37. V. V. Sagun and I. Lopes, Astrophys. J **2017**, 850, 75
38. P. Huovinen and P. Petreczky, Phys. Lett. B **2018**, 777, 125
39. V. Vovchenko, A. Motornenko, M. I. Gorenstein and H. Stoecker, Phys. Rev. C **2018**, 97, 035202
40. S. Typel, Eur. Phys. J. A **2016**, 52, 16
41. M. A. R. Kaltneborn, N. U. F. Bastian and D. B. Blaschke, Phys. Rev. D **2017**, 96, 056024
42. D. E. Alvarez-Castillo, D. B. Blaschke, A. G. Grunfeld and V. P. Pagura, arXiv:1805.04105 [hep-ph].
43. V. Paschalidis, K. Yagi, D. Alvarez-Castillo, D. B. Blaschke and A. Sedrakian, Phys. Rev. D **2018**, 97, 084038
44. H. Grigorian, D. N. Voskresensky and D. Blaschke, Eur. Phys. J. A **2016**, 52, 67
45. E. Annala, T. Gorda, A. Kurkela and A. Vuorinen, Phys. Rev. Lett. **2018**, 120, 172703
46. D. Vautherin and D. M. Brink, Phys. Rev. C **1972**, 5, 626

47. G. Röpke, D. Blaschke and H. Schulz, *Phys. Rev. D* **1986**, *34*, 3499
48. W. Ebeling, D. Blaschke, R. Redmer, H. Reinholz and G. Röpke, *J. Phys. A* **2009**, *42*, 214033
49. N. F. Carnahan and K. E. Starling, *J. Chem. Phys.* **1969**, *51*, 635
50. S. Typel and D. Blaschke, *Universe* **2018**, *4*, 32

© 2018 by the authors. Submitted to *MDPI* for possible open access publication under the terms and conditions of the Creative Commons Attribution (CC BY) license (<http://creativecommons.org/licenses/by/4.0/>).